A NEW SOLAR CURVE OF GROWTH

CHARLES R. COWLEY AND ANNE PYNE COWLEY
Yerkes Observatory
Received February 5, 1964; revised April 14, 1964

ABSTRACT

A solar curve of growth has been assembled using photoelectrically determined equivalent widths from the center of the disk obtained at the McMath-Hulbert Observatory. Six hundred and twelve lines of neutral Ca, Fe, Ti, V, Cr, Mn, and Co were used. Exclusive use has been made of the relative *f*-values obtained by Corliss and Bozman. The new system of *f*-values made it possible to treat lines of more elements over a wider range of excitation than earlier workers used. An excitation temperature of T_{ex} = 5143° K was found to be most appropriate to our data.

The lines of chromium cover almost the full extent of the curve of growth thus minimizing considerably the uncertainty sometimes met in fitting together the Doppler and damping portions of the curve of growth. The empirical curve agrees more closely with the van de Held curve of growth than with other theoretical curves based upon simple models. The new curve has also been compared to the empirical curves of growth of K. O. Wright and of Pierce and Goldberg.

The effect of variations of the continuous opacity with wavelength on the curve of growth has been assessed empirically. The results are only in qualitative agreement with previous results.

I. INTRODUCTION

In recent years it has become the practice to introduce more and more complexities into the treatment of the absorption lines formed in the solar atmosphere. Modern treatments have taken full account of the depth dependence of the temperature and pressure as well as possible inhomogeneities in the solar surface (multistream models), and have treated deviations from local thermodynamic equilibrium. In this paper we use a method based upon assumptions that were already old twenty years ago, and it would appear that some justification of this procedure is necessary.

Let us first point out that an enormous amount of work which makes use of "a" solar curve of growth has been, as is still being, done. The older curves of growth are based primarily upon the equivalent widths measured by C. W. Allen (1934, 1938) or on the measurements of the *Utrecht Atlas*. Both of these measurements are based exclusively on photographic photometry.

In constructing our curve of growth we have made use of equivalent widths from the center of the solar disk obtained by planimetry of photoelectric tracings made with the vacuum spectrograph of the McMath-Hulbert Observatory. The majority of these equivalent widths were most generously made available to us by Dr. E. A. Müller in advance of publication (Müller and Mutschlecner 1964). These lines are mainly the weak and medium-strong lines which outline the Doppler and "transition" regions of the curve of growth. We therefore found it necessary to obtain additional equivalent widths in order to outline the damping portion of the curve. The additional measurements came from two sources: (i) Our own measurements of the intermediate and strong lines from the McMath-Hulbert tracings.[1] The tracings were the same as those used by Dr. Müller so that reasonable agreement is to be expected. Figure 1 compares some of Dr. Müller's lines with our remeasurement. The agreement is entirely satisfactory. (ii) Equivalent widths given by Minnaert (1960). Almost all of the measurements of the stronger lines as published by Minnaert represent the weighted means of a number of determinations. Figure 2 shows the agreement between our measurements from the McMath-Hulbert photoelectric tracings and those of the Utrecht workers for the stronger lines.

We have made use entirely of the system of relative *f*-values of Corliss and Bozman (1962). These data represent an advance over those available to previous workers on two

[1] We would like to thank Dr. O. C. Mohler for making this material available to us.

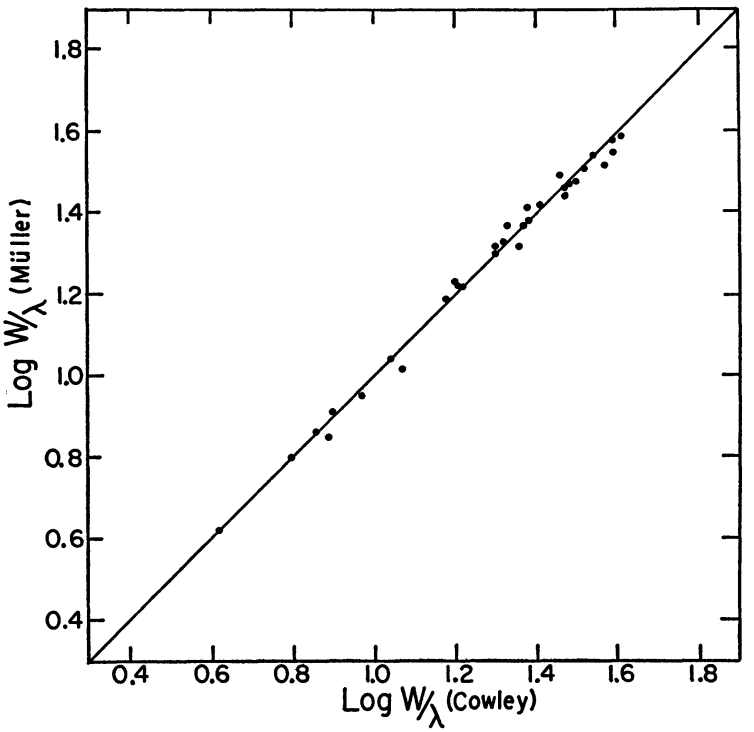

FIG. 1.—A comparison of the solar equivalent widths as measured from McMath-Hulbert Observatory photoelectric tracings of the center of the disk by E. A. Müller and by the writers.

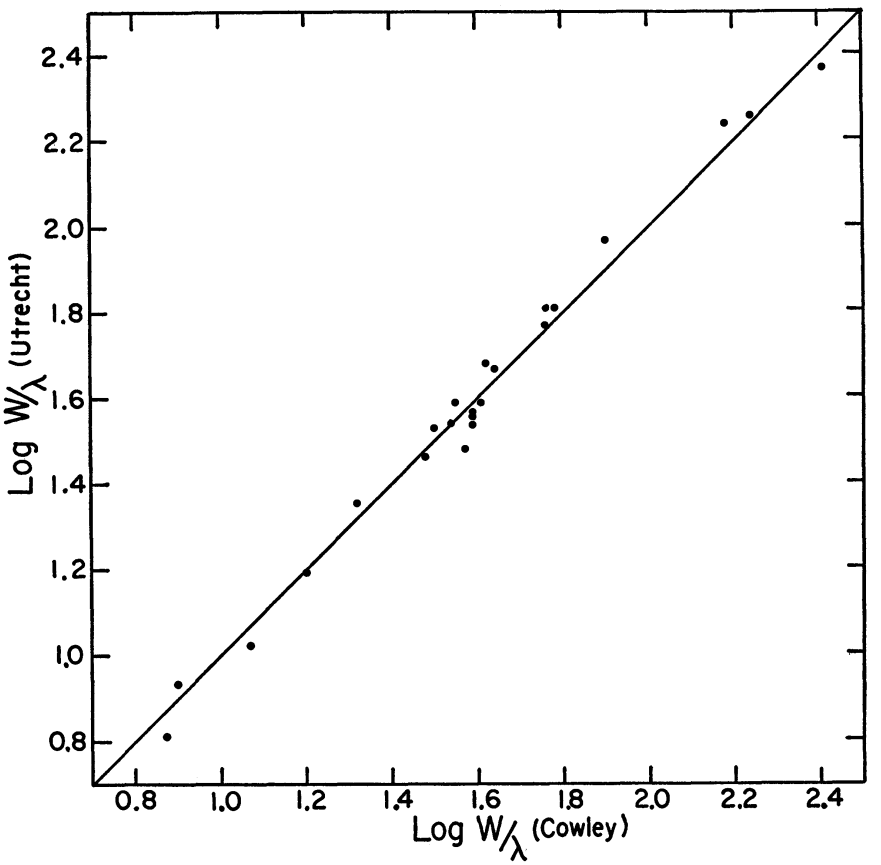

FIG. 2.—A comparison of the solar equivalent widths presented in the Utrecht publications and those measured by the writers for some of the strong lines.

accounts: (1) many lines of high excitation potential now have measured relative *f*-values, and (2) a large total number of lines for all the elements considered in this investigation is presented.

It might well be argued that the basic approach of the simple (Schuster-Schwarzschild [SS] or Milne-Eddington [ME]) curve of growth is somewhat dated, and that the advent of machine computation makes the detailed depth-dependent analysis the only realistic procedure in the quantitative analysis of stellar atmospheres.

The difficulties of the method of model atmospheres, however, are not merely computational. There are large uncertainties in the basic physical and astronomical data (*f*-values, effective temperatures, and surface gravities, etc.) There are, moreover, uncertainties in the theory of the depth-dependent treatment such as the importance of multistream effects or deviations from local thermodynamic equilibrium. The *grob* analysis is at present the only method available for the examination of abundances in a large number of stellar atmospheres. The rough treatment thus remains useful, in spite of its obvious shortcomings, and we feel that a new solar curve of growth based on improved data is well worthwhile.

II. PROCEDURE

Our curve of growth has been formed in the following manner. We first assumed a temperature $T = 5676°$ K (or $\theta = 0.888$) as suggested by Unsöld (1955). We then plotted $\log W/\lambda + 6.0 \equiv \log F$ against $\log gf\lambda - \theta\chi$, where χ is the excitation potential. Separate plots were made for lines arising from different levels of excitation. We then chose a new value of θ for each element by requiring that the scatter in the resulting curve of growth for that element be a minimum when all excitation levels were combined. A final mean θ was obtained by weighting the θ's derived from each element according to the number of lines used in the individual determination of θ. The resulting value was $\theta = 0.98$ which corresponds to a temperature of 5143° K.

The choice of an excitation temperature characterizing the entire solar atmosphere is somewhat problematical. In general, the higher-excitation lines show somewhat higher-excitation temperatures. Thus a temperature that would reduce the scatter for our Ti I lines, most of which arise from less than 2 eV, would increase the scatter for Mn I, where many of our lines arise from levels having an excitation greater than 2 eV. One must choose some mean excitation temperature which most nearly characterizes all of the lines used. Unsöld (1946, 1955) has emphasized that one must be careful to pick a value of θ which agrees with the high-excitation lines, since the error introduced into the abscissa of the curve of growth by an improper θ is less if χ is less.

The value of θ which we have adopted lies between that suggested by Unsöld (0.888) and the values employed by Pierce and Goldberg (1947) ($\theta = 1.08$) and Wright (1948) ($\theta = 1.04$ for Fe I, $\theta = 1.11$ for Ti I). The lower values of the temperature employed by Pierce and Goldberg and by Wright are undoubtedly due to the use of those lines for which there existed relative *f*-values measured in absorption by the Kings (1935, 1938) in an electric furnace. The lines that may be studied in this manner are mostly low-excitation lines, since it is difficult to observe high-excitation lines in absorption at the temperature of the Kings' furnace. On the other hand, the relative *f*-values of Corliss and Bozman extend to many more lines of high excitation than Kings' so that it is not at all surprising that we find our data require a somewhat higher temperature than did the data of Pierce and Goldberg or of Wright.

The somewhat higher-excitation temperature used by Unsöld resulted from the simultaneous determination of both the mean excitation-ionization temperature (LTE) and the electron pressure. The method is therefore substantially different from ours, and a further discussion of this determination is beyond the scope of this paper.

We should like to point out that any determination of the (mean) solar temperature using the lines of neutral atoms is tied directly to the determination of the temperature

in the arc or furnace in which the relative f-values were measured. One therefore determines in reality only the difference in the mean temperature of the Sun and the mean temperature of the arc or furnace. Our chosen value of the excitation temperature, $5040/\theta_{ex} = 5143°$ K, really means that the difference in the mean temperature of the solar atmosphere and of the copper arc of the National Bureau of Standards is small. Corliss chose a value of 5100° K for the NBS arc. If, for example, further study should show that 5200° K is a better value for the temperature of the NBS arc, then our excitation temperature ought also to be raised by 100° K.

In Table 1 we present the identification of the lines used in this investigation as well as the values of $\log F = \log W/\lambda + 6.0$ (where W is the equivalent width of the line) and $\log X = \log gf\lambda - \theta\chi$ (where gf is the value given by Corliss and Bozman). In order to make a composite curve of growth, it is necessary to superimpose in some way the curves defined by each element. It can be seen from inspection of Table 1 that the lines of chromium cover the whole range of the curve of growth and outline its general shape. The procedure has been to use the curve as defined by the chromium lines as a base around which the other curves have been assembled. Table 2 presents the relative shifts necessary to bring all of the abscissae into the system defined by the chromium lines.

The resulting composite curve of growth is displayed in Figure 3. The designation $\log X_{Cr}$ indicates that the abscissa is given in the chromium scale. Each point represents an individual line. Normal points in both coordinates were found, and a smooth curve was drawn through these. The solid line represents this mean curve of growth; it is defined by the values given in Table 3.

III. DISCUSSION

It is the usual practice to derive values of the Doppler width $\Delta\lambda_D$ and the damping constant Γ from a curve of growth. In order to do this, one compares the empirical curve of growth with some theoretical curve. Unfortunately there is no single, generally accepted theoretical curve of growth. Studies similar to the present one have made use of curves of growth based on very schematic model atmospheres which attempt to represent a large amount of equivalent-width data by a single curve. The detailed model solar atmospheres which take account of the depth dependence of the temperature and pressure have not generally been employed in the investigation of a turbulent velocity or a damping constant characteristic of the Sun as a whole. Indeed, the additional complexities which enter into the detailed depth-dependent treatment (uncertainties in the model and in the f-values, temperature inhomogeneities, etc.) have for the most part precluded an empirical investigation of the turbulent velocity and damping constant. This does not, of course, imply that a detailed depth-dependent treatment will have nothing to say on these questions, but only that the additional requirements upon the quality of the observational data are large.

The schematic models which have been traditionally employed are the Schuster-Schwarzschild (SS) and the Milne-Eddington (ME) atmospheres. For either of these models, slightly different curves of growth will result depending on whether the line-formation mechanism is taken to be (coherent) scattering or pure absorption. Unsöld (1955) recommends the use of an interpolation formula for the line depth R:

$$1/R = 1/R_0 + 1/x_\lambda\,, \tag{1}$$

where R_0 is the limiting or maximum-line depth (with the continuum taken as unity) and x_λ is proportional to the line-absorption coefficient. Depending on the choice of R_0, this formula may be made to fit line profiles sufficiently closely when formed either by pure absorption or scattering.

Our empirical curve of growth has been compared with theoretical curves from the four schematic models mentioned above, as well as Unsöld's "universal curve of growth,"

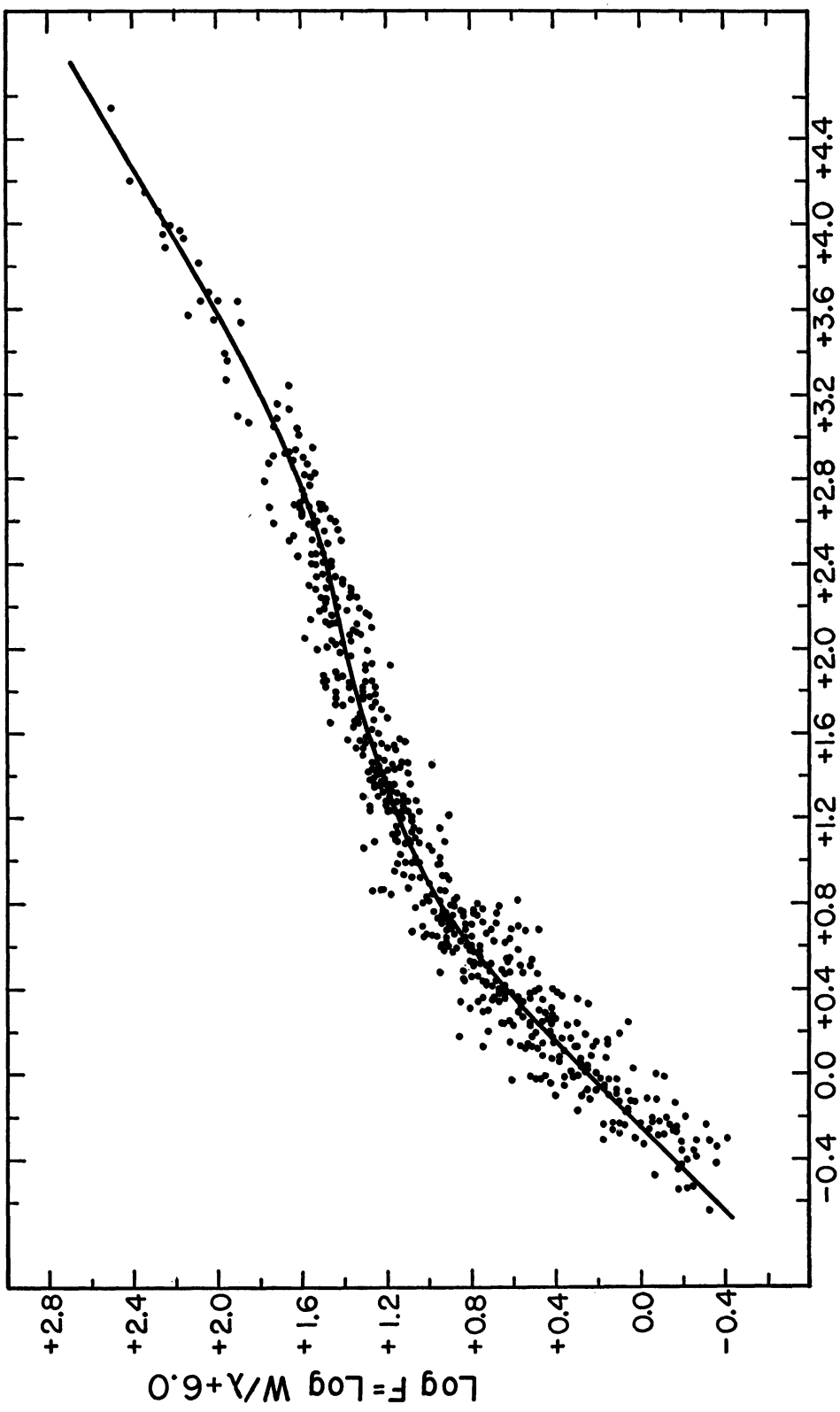

FIG. 3.—A new empirical solar curve of growth. Each point represents an individual line. The solid line is a mean curve drawn through the points given in Table 3.

TABLE 1

BASIC DATA FOR THE SOLAR CURVE OF GROWTH

Ca I

Multiplet	λ	log F	log X
1	6572.78	+0.58	-0.04
3	6102.72	+1.33	+1.33
4	4454.78	+1.62	+2.15
	4434.96	+1.61	+1.82
	4425.44	+1.53	+1.48
	4455.89	+1.46	+1.26
	4435.69	+1.49	+1.26
	4456.61	+1.23	00
5	4318.65	+1.48	+1.64
	4283.01	+1.54	+1.42
	4289.36	+1.51	+1.38
18	6439.07	+1.41	+1.65
	6493.78	+1.28	+1.30
	6471.66	+1.14	+0.71
	6499.65	+1.11	+0.70
19	6455.60	+0.91	+0.35
	6449.81	+1.19	+1.06
20	6169.56	+1.25	+0.96
	6169.06	+1.15	+0.66
	6166.44	+0.99	+0.59
	6161.29	+0.95	+0.29
	6163.76	+0.94	+0.29
21	5588.76	+1.43	+1.70
	5594.47	+1.37	+1.40
	5598.49	+1.34	+1.22
	5601.28	+1.32	+0.93
	5581.97	+1.25	+0.93
	5590.12	+1.23	+0.85
22	5265.56	+1.39	+1.32
	5261.71	+1.28	+0.92
23	4578.56	+1.28	+0.38
32	6717.68	+1.21	+0.40
33	5349.47	+1.27	+1.07
34	5041.62	+1.32	+0.67
36	4526.94	+1.32	+0.20
47	5857.45	+1.37	+1.39
48	5512.98	+1.22	+0.46

Ti I

Multiplet	λ	log F	log X
3	5460.50	+0.19	+1.33
	5426.26	+0.05	+1.23
	5490.84	-0.36	+1.02
4	5210.39	+1.22*	+2.77
	5192.97	+1.21	+2.74
	5173.74	+1.12	+2.65
	5219.70	+0.68	+1.80
	5152.18	+0.82	+1.96
	5147.48	+0.83	+2.00
5	5064.65	+1.25	+2.78
	5039.96	+1.17	+2.72
	5009.65	+0.64	+1.72
	4997.10	+0.73	+1.80
6	4681.91	+1.18*	+2.63
	4656.47	+1.16	+2.52
7	4562.64	+0.32	+1.36
9	4112.71	+0.98	+2.12
11	3982.48	+1.16	+2.59

Ti I - Continued

Multiplet	λ	log F	log X
12	3998.64	+1.50	+3.71
	4024.57	+1.35	+2.89
	3964.27	+1.10	+2.82
	3962.85	+1.12	+2.82
35	5366.65	-0.41	+1.05
	5389.18	-0.03	+1.25
37	5238.56	+0.46	+1.71
	5246.57	-0.07	+1.36
38	4981.73	+1.36	+3.45
	4991.07	+1.36	+3.34
	4999.50	+1.30	+3.28
	5016.16	+1.10	+2.44
	5020.03	+1.20	+2.60
	5022.87	+1.19	+2.60
	5024.84	+1.09	+2.44
42	4533.24	+1.34	+3.48
	4534.79	+1.30*	+3.26
	4535.92	+1.29	+2.78
	4536.05	+1.20	+2.78
	4555.49	+1.13	+2.56
	4548.76	+1.20	+2.68
	4512.73	+1.16	+2.59
	4518.02	+1.19	+2.72
	4527.30	+1.20	+2.59
43	4326.36	+0.76	+1.95
44	4287.40	+1.18	+2.68
	4286.01	+1.26	+2.71
	4281.37	+0.73	+1.79
48	6743.12	+0.37	+1.53
49	6599.11	+0.07	+1.18
69	6064.63	+0.06	+1.60
71	5880.31	+0.04	+1.39
72	5866.45	+0.87	+2.19
	5899.30	+0.65	+1.95
	5922.11	+0.49	+1.75
	5941.76	+0.41	+1.64
74	5295.78	+0.28	+1.43
77	4675.12	+0.87*	+1.53
80	4060.26	+0.92	+2.43
102	6556.07	+0.38	+1.44
	6554.23	+0.33	+1.37
104	6258.71	+0.89	+2.16
	6258.10	+0.88	+2.15
	6261.10	+0.89*	+2.05
106	5512.53	+0.90*	+2.15
	5514.54	+0.89	+2.11
	5514.35	+0.80	+2.06
	5481.86	+0.30	+1.49
110	5036.47	+1.13	+2.59
	5038.40	+1.08	+2.55
126	4820.41	+0.92*	+1.98
145	4617.27	+1.15	+2.67
	4623.10	+1.07*	+2.37
	4639.67	+0.92	+2.03
	4639.37	+0.91	+2.06
146	4465.81	+0.88	+2.18
	4471.24	+0.97*	+2.09
154	5953.16	+0.69	+2.06
	5965.83	+0.64	+1.90
	5978.54	+0.54	+2.03
156	5297.24	+0.56	+1.70

TABLE 1 Continued

Ti - Concluded

Multiplet	λ	log F	log X
157	4885.08	+1.08	+2.28
	4899.91	+1.05	+2.28
	4913.62	+1.01	+2.19
160	4450.90	+1.07*	+2.47
233	4759.27	+0.99*	+2.20
240	5644.14	+0.73*	+2.02

V I

Multiplet	λ	log F	log X
3	4881.55	+1.04*	+2.49
	4875.46	+0.94	+2.41
	4864.74	+0.79	+2.31
	4851.48	+0.86*	+2.14
	4827.46	+0.43	+1.75
	4831.65	+0.52	+1.79
	4832.43	+0.40	+1.70
4	4594.10	+1.08	+2.79
	4586.36	+0.95	+2.61
	4580.39	+0.94	+2.50
	4577.17	+0.80	+2.40
5	4352.87	+1.17	+2.75
	4332.83	+0.88	+2.46
	4330.02	+0.85	+2.42
19	6243.11	+0.62*	+2.34
	6251.83	+0.31	+1.93
	6256.91	-0.26	+1.42
	6296.52	+0.06	+1.71
	6292.86	+0.31	+1.78
	6285.18	+0.15	+1.78
	6274.67	+0.11	+1.71
	6199.20	+0.25	+2.13
	6216.37	+0.67	+2.14
	6242.80	+0.11	+1.72
20	6150.13	+0.17	+1.75
	6213.87	-0.12	+1.59
	6224.51	-0.09	+1.58
	6233.19	-0.19	+1.48
21	4459.76	+1.11	+2.73
	4437.84	+0.84	+2.54
	4441.68	+1.27*	+2.66
	4444.21	+0.92	+2.54
	4419.94	+0.21	+1.80
	4436.14	+0.93	+2.38
22	4379.24	+1.41	+3.83
	4384.72	+1.44	+3.59
	4389.97	+1.36*	+3.43
	4400.58	+1.10	+2.89
	4406.64	+1.32	+3.10
	4408.20	+1.24	+3.29
	4408.51	+1.24	+3.40
	4426.00	+0.91*	+2.40
	4421.57	+0.94	+2.54
	4416.47	+0.97	+2.53
24	4189.59	+0.64	+2.04
27	4111.78	+1.37	+3.77
	4115.18	+1.34	+3.45
	4116.47	+1.12	+3.08
	4105.17	+1.27	+3.26
34	6090.18	+0.67	+2.59
	6119.50	+0.49	+2.27

V I - Concluded

Multiplet	λ	log F	log X
34	6135.36	+0.15	+1.94
	6039.69	+0.30	+2.15
	6081.42	+0.37	+2.17
	6111.62	+0.21	+1.95
	6058.11	-0.26	+1.49
35	5727.02	+0.80*	+2.44
	5698.51	+0.77	+2.60
	5703.56	+0.70	+2.48
	5743.44	+0.08	+1.56
	5737.04	+0.17	+1.87
	5727.66	+0.17	+1.74
36	5670.83	+0.43	+2.00
37	5627.63	+0.57	+2.12
	5626.01	-0.25	+1.27
	5668.37	-0.13	+1.56
	5657.45	00	+1.57
	5646.11	-0.25	+1.44
	5584.49	-0.08	+1.68
	5592.41	-0.11	+1.52
	5604.94	-0.19	+1.37
48	6531.44	-0.04	+1.54
	6452.35	-0.07	+1.33
52	4113.52	+0.39	+2.19
62	4501.97	+0.21	+1.79
87	4452.01	+0.78	+2.54
	4469.71	+0.75	+2.32
	4468.01	+0.26	+1.81
88	4268.64	+0.93	+2.54
	4277.96	+0.99	+2.45
89	3990.57	+1.00	+2.61
	3988.83	+0.28	+1.83
92	5772.40	-0.36	+1.38
99	4524.22	+0.23	+1.89
101	4457.76	+0.33	+1.81
109	4571.78	+0.60	+2.03
	4578.73	+0.42	+1.87
110	4474.04	+0.10	+1.99
112	4104.78	+0.75	+2.24
113	4807.54	+0.47	+1.78
	4796.93	+0.30	+1.78
119	4710.57	-0.05	+1.58
121	4057.07	+0.57	+2.31
129	5487.92	+0.18	+1.49
131	5240.88	+0.06	+1.64
	5234.09	+0.06	+1.63

Cr I

Multiplet	λ	log F	log X
1	4254.35	+1.96†	+3.36
	4274.80	+1.66†	+3.24
	4289.72	+1.73†	+3.05
6	6330.10	+0.58	+0.36
7	5208.44	+1.68†	+2.92
	5206.04	+1.56†	+2.81
8	5072.92	+0.79	+0.52
9	4964.93	+0.84	+0.48
10	4496.86	+1.30	+1.82
	4545.96	+1.28	+1.77
	4580.06	+1.27	+1.54
18	5409.79	+1.43†	+2.02

TABLE 1 - Continued

Cr I - Continued

Multiplet	λ	log F	log X
18	5296.69	+1.24	+1.90
	5300.75	+1.03	+0.80
	5247.56	+1.18	+1.34
20	5123.46	+0.49	+0.12
21	4646.17	+1.30	+2.17
	4652.16	+1.29	+1.90
	4600.75	+1.26	+1.66
	4591.39	+1.17	+1.54
	4613.37	+1.21	+1.35
22	4351.05	+1.32	+1.56
	4412.25	+0.79	+0.57
	4373.25	+1.00	+0.89
30	4885.78	+0.73	+0.51
31	4789.35	+1.12	+1.25
	4829.38	+1.15	+0.99
32	4571.68	+0.93	+1.09
	4637.18	+0.69	+0.62
	4648.13	+0.67	+0.38
	4649.46	+0.76	+0.55
33	4529.85	+0.64	+0.40
	4541.07	+0.76	+0.58
	4535.15	+0.83	+0.70
	4539.79	+0.92	+0.64
35	4126.52	+1.06	+1.28
	4203.59	+1.10	+0.87
37	4026.17	+1.05	+1.23
38	3984.34	+1.18	+1.45
59	5238.97	+0.51	+0.18
60	5110.75	+0.67	+0.39
61	4745.31	+0.40	+0.26
62	4697.06	+0.79	+0.75
	4700.61	+0.51	+0.53
64	4295.76	+1.11	+0.99
	4381.11	+0.92	+0.73
65	4120.61	+0.68	+0.75
66	4077.09	+0.79	+0.76
67	3992.84	+1.24	+1.44
	3978.68	+1.26	+1.09
81	4619.55	+0.92	+0.86
	4501.79	+0.75	+0.36
	4622.76	+0.64	+0.38
	4501.11	+0.89	+0.71
	4498.73	+0.75	+0.71
	4432.18	+0.93	+0.73
99	4693.95	+0.75	+0.77
	4695.15	+0.53	+0.37
104	4346.83	+0.94	+0.93
119	5719.82	-0.17	-0.27
127	4458.54	+1.05	+1.08
	4465.36	+0.71	+0.52
143	4922.27	+1.22	+1.37
	4887.01	+1.11	+1.08
	4870.80	+1.17	+1.12
	4885.96	+0.42	+0.24
144	4836.86	+0.55	+0.12
145	4737.35	+1.08	+1.15
	4730.71	+1.00	+1.06
	4724.42	+0.83	+0.68
147	4656.19	+0.73	+0.30
150	4540.72	+1.10	+1.41
	4511.90	+0.95	+1.01
166	4954.81	+0.96	+0.98
	4936.33	+0.95	+0.99

Cr I - Concluded

Multiplet	λ	log F	log X
168	4801.03	+0.99	+1.05
170	4680.87	+0.75	+0.29
186	4718.43	+1.16	+1.37
	4708.04	+1.10	+1.28
	4689.37	+0.93	+0.86
	4669.34	+0.91	+0.68
	4666.51	+0.94	+0.86
	4664.80	+1.05	+0.99
188	5787.99	+0.80	+0.64
	5785.82	+0.62	+0.15
	5785.00	+0.66	+0.24
	5783.93	+0.77	+0.34
	5783.11	+0.62	+0.48
191	5405.00	+0.35	+0.23
	5386.98	+0.61	+0.38
193	5221.75	+0.70	+0.41
	5214.13	+0.51	+0.22
196	4526.11	+0.54	+0.14
201	5243.40	+0.48	+0.40
	5177.43	+0.55	+0.48
	5200.19	+0.66	+0.49
203	5702.31	+0.62	+0.26
	5628.64	+0.43	+0.26
204	5480.50	+0.26	+0.19
	5442.41	+0.20	-0.02
206	5193.49	+0.36	-0.01
225	5272.01	+0.71	+0.48
	5287.19	+0.28	-0.10
	5304.21	+0.46	+0.14
	5312.88	+0.48	+0.30
	5318.78	+0.42	+0.31
	5344.76	+0.15	-0.10
	5340.44	+0.47	+0.08
231	4767.86	+0.50	+0.39
233	4622.49	+0.94	+0.76
234	4413.87	+0.81	+0.58
239	5694.73	+0.52	+0.23
	5642.36	+0.03	-0.30
	5649.37	+0.25	-0.07
243	5746.43	-0.18	-0.54
247	4263.14	+1.07	+0.78
248	4209.37	+0.84	+0.76
249	4208.36	+0.58	+0.29
251	4039.10	+1.06	+0.99
261	4131.36	+0.70	+0.35
	4152.78	+0.72	+0.20
272	4204.47	+0.56	+0.27
282	6661.08	+0.22	+0.13
	6669.26	-0.08	-0.12

Mn I

Multiplet	λ	log F	log X
5	4055.54	+1.48	+1.99
	4070.28	+1.22	+1.17
	4018.10	+1.52	+1.88
	4035.73	+1.50	+1.89
	4058.93	+1.36	+1.74
	4083.63	+1.46	+1.74
	4082.94	+1.37	+1.73
	4079.42	+1.41	+1.57

TABLE 1 - Continued

Mn I - Concluded

Multiplet	λ	log F	log X
16	4823.52	+1.50	+1.57
	4783.42	+1.48	+1.55
	4754.04	+1.44	+1.59
20	4965.88	+0.83	+0.13
	5004.91	+0.41	-0.15
21	4762.38	+1.37	+1.46
	4766.43	+1.30	+1.28
	4765.86	+1.21	+1.06
	4761.53	+1.15	+0.83
	4709.72	+1.10	+0.80
	4739.11	+1.07	+0.69
	4671.69	+0.41	+0.10
22	4451.59	+1.32	+1.52
	4464.68	+1.28	+1.08
	4470.14	+1.10	+0.93
	4414.88	+1.25	+1.16
	4436.35	+1.21	+0.97
	4453.00	+1.05	+0.84
	4502.22	+1.15	+0.98
	4498.90	+1.12	+0.99
23	4235.29	+1.33	+1.39
	4235.14	+1.23	+1.25
	4239.72	+1.28	+0.95
	4281.10	+1.26	+1.09
	4265.92	+1.17	+1.13
	4257.66	+1.14	+1.14
27	6021.80	+1.18	+0.94
	6016.64	+1.15	+0.78
	6013.50	+1.12	+0.63
28	4458.26	+1.23	+1.05
	4461.08	+1.16	+0.79
	4457.55	+1.20	+0.95
	4457.04	+0.97	+0.35
29	4059.39	+1.14	+0.83
	4057.95	+1.18	+1.00
32	5255.32	+0.85	+0.46
	5196.59	+0.81	+0.23
	5117.94	+0.63	+0.33
39	6440.97	-0.11	-0.31
42	5377.63	+0.93	+0.45
	5399.49	+0.84	+0.14
	5413.69	+0.57	+0.02
43	4844.32	+0.36	-0.19
47	4105.36	+0.50	-0.32
48	4049.00	+0.75	-0.17
	4055.21	+0.67	+0.09

Fe I

Multiplet	λ	log F	log X
1	5110.41	+1.44	+0.46
2	4375.93	+1.54*	+1.07
	4427.31	+1.59*	+1.06
	4461.65	+1.46*	+0.75
	4482.17	+1.55	+0.74
3	4216.19	+1.50	+0.53
4	3922.91	+2.09†	+2.16
	3930.30	+2.26†	+2.29
	3927.93	+2.16†	+2.27
	3920.26	+2.00†	+1.98
15	5328.04	+1.85†	+1.41

Fe I - Continued

Multiplet	λ	log F	log X
15	5371.49	+1.64†	+1.23
	5405.78	+1.60*	+0.98
	5434.53	+1.52*	+0.83
	5397.13	+1.60*	+0.99
	5446.92	+1.54*	+0.91
	5501.47	+1.32*	+0.14
	5506.78	+1.33*	+0.43
16	5051.64	+1.38	+0.18
	5083.34	+1.31	+0.09
36	5171.60	+1.47	+0.95
	5194.94	+1.41	+0.65
	5216.28	+1.37*	+0.57
37	5227.19	+1.73†	+1.25
	5328.53	+1.49	+0.56
39	4602.94	+1.41*	+0.66
	4531.15	+1.44	+0.58
41	4383.55	+2.41*	+2.54
	4404.75	+2.24*	+2.23
	4415.12	+1.90*	+1.98
	4337.05	+1.57*	+0.93
42	4271.76	+2.25†	+2.34
	4307.91	+2.22†	+2.33
	4325.76	+2.18*	+2.31
	4202.03	+1.89†	+1.88
	4250.79	+1.96†	+1.73
	4147.67	+1.44	+0.68
43	4045.82	+2.50†	+2.88
	4063.60	+2.34†	+2.48
	4071.74	+2.28†	+2.40
	4005.25	+2.04†	+2.02
	4143.87	+2.08†	+1.98
	4132.06	+2.02†	+1.89
62	6430.85	+1.25	+0.09
	6265.14	+1.13	-0.20
68	4528.62	+1.63†	+1.28
	4494.57	+1.59*	+1.06
	4442.34	+1.61*	+1.00
	4447.72	+1.56	+1.01
71	4282.41	+1.60	+1.24
	4315.09	+1.56	+1.11
	4352.74	+1.53	+0.94
72	3977.74	+1.58	+1.21
111	6421.36	+1.20*	+0.01
	6945.21	+1.09	-0.30
	6978.86	+1.10	-0.43
114	5049.82	+1.46	+0.50
152	4260.48	+2.14†	+1.91
	4235.94	+1.96†	+1.81
	4222.22	+1.60	+0.96
	4187.80	+1.72	+1.49
	4191.44	+1.66	+1.27
	4250.12	+1.90†	+1.44
	4271.16	+1.72†	+1.43
	4233.61	+1.85†	+1.41
168	6494.98	+1.38	+0.58
	6393.60	+1.32*	+0.10
	6318.02	+1.27	-0.20
169	6252.56	+1.27	+0.19
	6191.56	+1.32	+0.41
	6136.62	+1.34	+0.59
207	6230.73	+1.38*	+0.40
	6137.70	+1.33	+0.41
	6065.49	+1.30*	+0.19

TABLE 1 - Continued

Fe I - Concluded

Multiplet	λ	log F	log X
268	6677.99	+1.29	+0.34
	6592.92	+1.27	+0.06
	6546.24	+1.20	-0.13
277	3971.32	+1.55	+0.85
278	4021.87	+1.52	+1.02
	3981.78	+1.50	+0.75
318	4891.50	+1.78*	+1.13
	4871.32	+1.64*	+1 02
	4919.00	+1.73†	+0.93
	4890.76	+1.62*	+0.78
	4872.14	+1.55*	+0.78
350	4443.20	+1.37*	+0.62
354	4181.76	+1.55	+1.29
	4175.64	+1.44	+0.94
	4156.80	+1.51	+1.00
	4107.49	+1.50	+1.01
355	4154.50	+1.49	+1.00
357	4134.68	+1.50	+1.01
359	4062.45	+1.49	+0.90
383	5232.95	+1.76*	+1.22
	5266.56	+1.64*	+0.87
	5192.35	+1.55	+0.97
	5068.77	+1.43	+0.20
	5191.46	+1.50	+0.79
518	4369.77	+1.56*	+0.48
522	4199.10	+1.66	+1.47
553	5324.18	+1.76*	+1.01
	5283.63	+1.54*	+0.78
	5393.17	+1.47*	+0.47
	5339.94	+1.48*	+0.35
	5302.31	+1.48	+0.58
554	4736.78	+1.48	+0.46
686	5615.65	+1.66	+0.85
	5572.85	+1.57*	+0.64
	5569.62	+1.47	+0.45
	5576.10	+1.35	00
	5624.55	+1.38	+0.16
693	4227.43	+1.63	+1.38
	4247.43	+1.54	+0.74
801	4118.55	+1.59	+1.04
816	6400.01	+1.42	+0.32
	6411.66	+1.32	+0.11
	6246.33	+1.27	-0.04
	6301.52	+1.30*	-0.11
965	5001.87	+1.49	+0.16
984	5005 72	+1.41	+0.07
1107	5762.99	+1.24	-0.16
1146	5383.37	+1.59*	+0.39
	5369.96	+1.50*	+0.18
	5367.47	+1.47*	-0.01
	5364.87	+1.39	-0.09
1163	5445.04	+1.33	-0.09
1165	5415.20	+1.53	+0.34
	5410.91	+1.44	+0.08
1178	6024.07	+1.27*	-0.23

Co I

Multiplet	λ	log F	log X
1	4190.71	+1.08	+0.97
	4252.30	+0.77	+0.76

Co I - Continued

Multiplet	λ	log F	log X
3	3979.52	+1.19	+1.14
	4027.03	+0.93	+0.90
16	4020.90	+1.24	+1.60
	3952.33	+0.80	+0.76
	4019.29	+0.57	+0.43
18	3957.93	+1.14	+1.41
28	4121.32	+1.46	+2.69
	4118.77	+1.43	+2.50
29	4092.39	+1.35	+1.97
	4110.53	+1.32	+1.79
30	4066.36	+1.20	+1.60
31	3995.31	+1.48	+2.86
32	3997.90	+1.44	+2.07
37	6189.00	+0.15	+0.27
	6093.14	+0.10	+0.17
38	5530.78	+0.37	+0 47
39	5483.35	+0.89	+0.87
	5369.59	+0.95	+0.78
	5331.46	+0.45	+0.59
	5301.04	+0.53	+0.66
	5230.21	+0.70	+0.98
	5247.92	+0.48	+0.98
55	5935.39	-0.33	-0.01
58	4068.54	+0.91	+1.21
	4058.60	+0.90	+0.98
81	6429.91	-0.24	-0.10
82	5890.49	-0.11	+0.29
90	5590.74	+0.20	+0.43
92	4899.52	+0.27	+0.33
112	5647.23	+0.33	+0.47
113	3977.18	+0.63	+0.55
142	4543.81	+0.64	+0.71
143	4431.61	+0.15	+0.20
150	4530.95	+1.14	+1.33
	4469.55	+1.01	+0.96
	4471.55	+0.46	+0.55
	4478.32	+0.46	+0.29
	4421.34	+0.61	+0.27
156	4749.68	+0.87	+0.89
	4771.11	+0.64	+0.77
	4768.07	+0.36	+0.24
	4754.36	+0.30	+0.13
	4734.83	+0.10	+0.07
	4693.19	+0.63	+0.83
158	4867.87	+1.08	+1.50
	4813.48	+0.97	+1.06
	4792.86	+0.93	+1.23
	4882.70	+0.15	+0.46
165	6086.66	-0.31	+0.06
166	5495.68	-0.22	-0.10
169	6000.67	-0.16	+0.16
170	5212.70	+0.58	+1.00
	5146.75	+0.52	+0.81
	5122.77	+0.50	+0.49
172	5352.05	+0.61	+0.98
	5280.63	+0.58	+0.89
	5266.30	+0.69	+0.66
173	3991.53	+0.81	+0.61
174	6455.00	+0.30	+0.54
	6595.87	-0.16	+0.04
	6477.86	-0.21	+0.10
175	5470.46	+0.03	+0.17
	5452.30	-0.17	+0.05

TABLE 1 - Concluded

Co I - Continued

Multiplet	λ	log F	log X
175	5287.57	-0.05	+0.09
176	4594.63	+0.42	+0.47
	4625.77	+0.13	+0.04
177	4596.90	+0.51	+0.43
178	4570 02	+0.13	+0.07
180	5156.37	+0.25	+0.34
181	5108.90	+0.24	+0.18
187	5287.78	-0.08	+0.01
190	5342.70	+0.75	+0.86
	5250.00	+0.18	+0.06
	5333.65	+0.10	+0.02

Co I - Concluded

Multiplet	λ	log F	log X
192	5325.28	+0.25	+0.33
	5524.99	-0.19	-0.06
194	5359.20	+0.21	+0.22
	5325.95	-0.22	-0.24
195	5454.57	+0.38	+0.37
196	5444.58	+0.41	+0.47
	5381.78	-0.01	-0.03
	5347.50	-0.20	-0.08
	5310.22	-0.33	-0.33
197	5312.65	+0.11	+0.27
200	6347.84	-0.18	-0.15

*Cowley measurement
†Utrecht measurement

TABLE 2

RELATIVE HORIZONTAL SHIFTS OF THE ELEMENTS*

Element	Δ log X	Element	Δ log X
Ca	+0.86	Mn	+0.30
Ti	-1.36	Fe	+1.66
V	-1.80	Co	-0.30

*If Δ log X is added to the abscissa of the curve of growth for any element, the resulting curve will superimpose on that of chromium.

TABLE 3

MEAN EMPIRICAL CURVE OF GROWTH

$\log X_{Cr}$	$\log \frac{W}{\lambda} + 6.0$	$\log X_{Cr}$	$\log \frac{W}{\lambda} + 6.0$
-0.40	-0.16	+2.20	+1.44
-0.20	+0.04	+2.40	+1.49
00	+0.24	+2.60	+1.55
+0.20	+0.44	+2.80	+1.62
+0.40	+0 63	+3.00	+1.70
+0.60	+0 79	+3 20	+1.79
+0.80	+0.93	+3.40	+1.89
+1.00	+1.05	+3.60	+2.00
+1.20	+1.15	+3 80	+2.11
+1.40	+1.22	+4 00	+2.23
+1.60	+1.29	+4.20	+2.35
+1.80	+1.34	+4.40	+2.46
+2.00	+1 39	+4.60	+2.58

which is based upon the interpolation formula in equation (1). Theoretical curves have been taken from the following sources:

ME-scattering: Wrubel (1950)
SS-scattering: Wrubel (1954)
ME–pure absorption: Hunger (1956)
SS–pure absorption: van de Held (1931)
Interpolation formula: ten Bruggencate and Houtgast (1941).

All of these curves begin with the usual 45° or straight-line portion for the weak lines and end with the damping or $\sim \sqrt{N}$-portion for the strongest lines. Between these is the "transition" region; the five curves listed above differ only in this transition region. The manner in which the theoretical points leave the transition region and enter the damping portion is governed by a free parameter, the damping constant Γ, which is to be determined empirically. We find, as did Pierce and Goldberg, that our strongest lines may not be fit by a single value of the camping constant (i.e., for large equivalent widths our empirical curve rises with a slope greater than $\frac{1}{2}$). We thus find that the only empirical justification for a choice of one theoretical curve over another is the shape of the "shoulder" (the region bridging the Doppler and transition portions) of the empirical curve of growth.

Our empirical curve agrees most closely with the theoretical curves of van de Held (see Fig. 4), and we have consequently derived values of the "mean" damping constant Γ and the turbulent velocity ξ_t from these curves. So many approximations are made in any of the simple curve-of-growth procedures that we would hesitate to draw any firm conclusions concerning the nature of the formation of the Fraunhofer lines from the agreement of the van de Held curves with our empirical one. Nevertheless, if we assume that the excitation temperature equals the gas kinetic temperature, we obtain a turbulent velocity of 1.4 km/sec with an uncertainty of about 0.2 km/sec. This value is in good agreement with previous determinations of the microturbulent velocity from line profiles (de Jager, 1959). One should, however, use care in the intercomparison of published values of the microturbulent velocity determined by "the" curve of growth procedure, since the published values depend both upon the assumed temperature *and* the curve of growth chosen to represent the data. Our value of $\xi_t = 1.4$ is in satisfactory agreement with the data of Wright and of Pierce and Goldberg if we use the van de Held curve and our excitation temperature to find ξ_t from their empirical curves.

A comparison of our results with the van de Held curves also yields a value of 1.4 for the logarithm of the ratio of the observed to the classical damping constant. This value is in agreement with the average values that have been found by previous workers. (see Minnaert 1953).

Our curve of growth agrees well with the empirical curve of Wright's (1948) in the Doppler and transition regions (see Fig. 5). However, our curve turns up sooner into the damping or square-root portion. The linear extent of the "flat" or transition region of Wright's curve was determined by the fit of the iron lines to the titanium. Naturally this fit is complicated by the fact that Wright's iron lines lie primarily in the damping portion of the curve of growth while his titanium lines lie in the Doppler and transition regions. Pierce and Goldberg made use of vanadium lines in addition to those of iron and titanium, but their vanadium lines, like those of titanium, lie primarily on the Doppler and transition regions. On the other hand, the chromium lines, which outline most of our curve of growth, have forced us to conclude that the transition region is in fact rather small.

Our data show, in qualitative agreement with the work of Pierce and Goldberg, that the damping portion of the empirical curve of growth is not linear with a slope of $\frac{1}{2}$. This result could be due to a number of causes. Four possibilities are given: (i) the damping constant is different for different lines; (ii) the wavelength dependence of the ab-

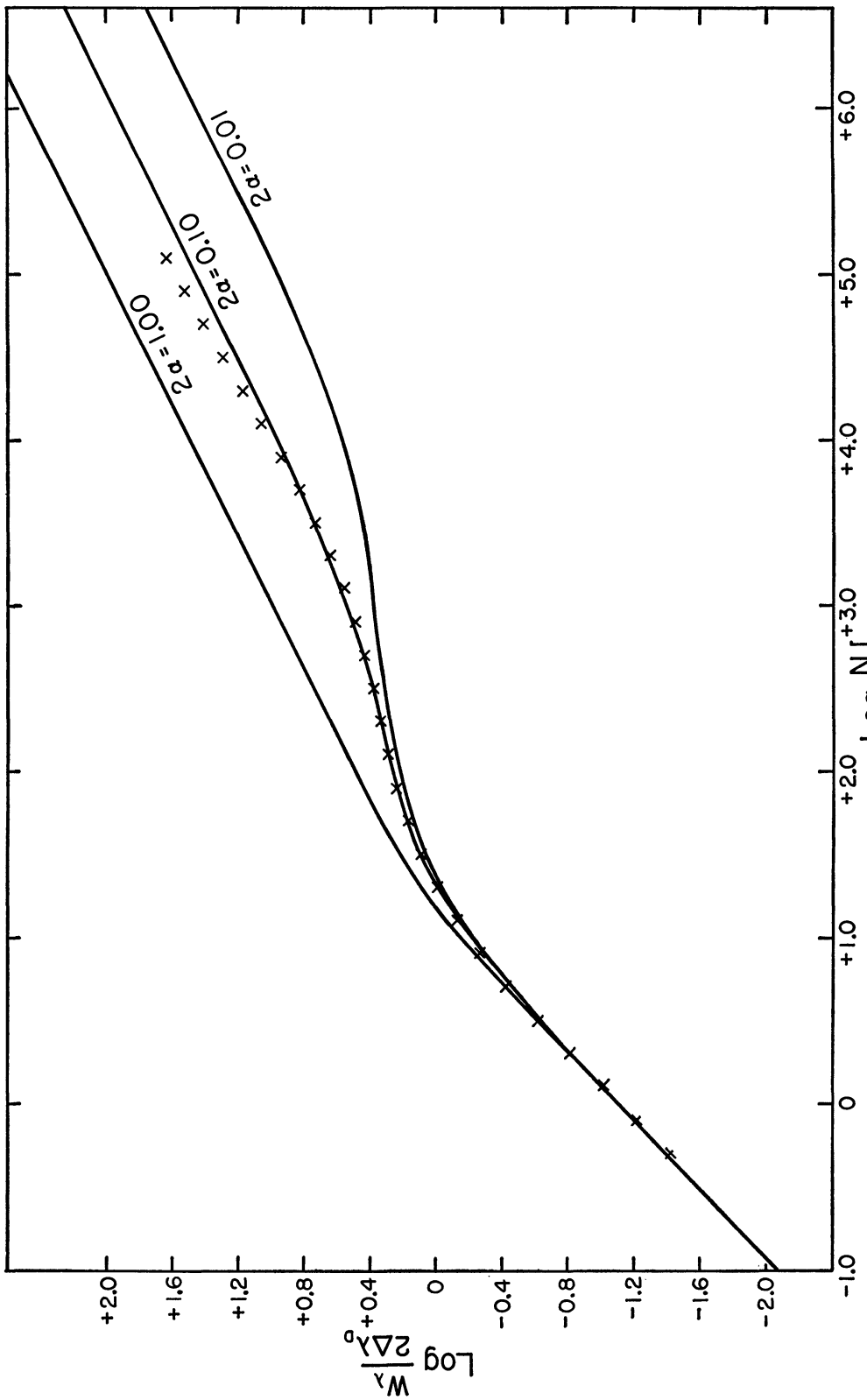

FIG. 4.—Empirical and theoretical curves of growth. The solid lines represent the theoretical curve of growth given by van de Held. Crosses outline the mean curve shown in Fig. 3.

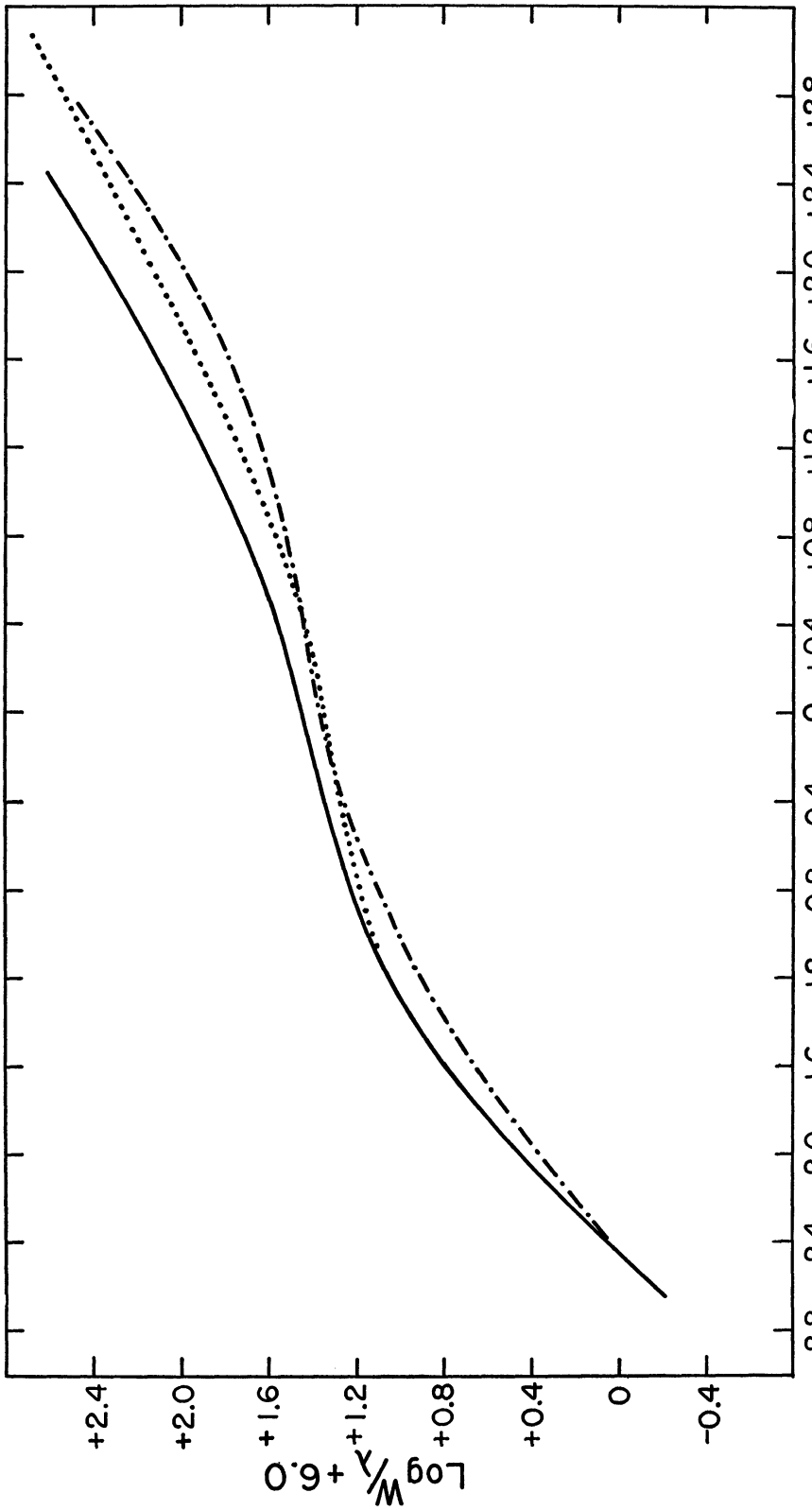

FIG. 5.—Comparison of the empirical curves of growth of Pierce and Goldberg (*dots and dashes*), Wright (*dotted line*), and the writers (*solid line*). The three curves were arbitrarily made to coincide at the straight-line, or Doppler, portion of the curve of growth.

sorption coefficient is proportional to $\Delta\lambda^{-n}$ with $n \neq 2$ in the wings of the lines (Unsöld 1955); (iii) self-reversal of the strongest lines in the NBS arc was not entirely eliminated in the determination of the relative f-values; (iv) systematic photometric errors.

On theoretical grounds one would expect that the first two factors would be of some influence. However, with the exception of hydrogen and helium lines, it has generally been assumed that these effects are small, at least in the *grob* approximation. Self-reversal of emission lines is a well-known source of error in the determination of relative f-values, and consequently every attempt is made by workers in this field to eliminate or allow for the phenomenon (Corliss and Bozman 1962). The effect is mentioned because it is in the expected direction, i.e., the strongest lines would be most strongly self-reversed, and this would result in larger observed damping constants for the strongest solar lines as these lines are also strongest in the arc.

On the other hand, Pierce and Goldberg made use of Kings' f-values obtained in absorption where self-absorption would act in the opposite sense to self-reversal in the arc. Therefore it is not possible to explain the upturn of the Pierce-Goldberg curve of growth in the same way. However, the Kings (1938) mention the following systematic effect pointed out by Minkowski. There is a tendency to draw the continuum too high on the photometric tracing of the absorption lines observed in the electric furnace. This effect would act to increase the gf-values of the weaker lines relative to the stronger ones.

Let us now consider the effect of the variability of the continuous-absorption coefficient with wavelength. A realization that such variation could affect curves of growth was perhaps an important factor in the preference by many workers for the Milne-Eddington over the Schuster-Schwarzschild atmosphere, since in the former the expression for the continuous-absorption coefficient appears explicitly in the abscissa of the curve of growth. The variation of the continuous opacity with wavelength may also be accounted for in the Schuster-Schwarzschild model by allowing for changes in the effective thickness, H, of the line-forming region (Unsöld 1955).

The variation of the continuous opacity was investigated empirically by ten Bruggencate (1944) and by Pierce and Goldberg (1947); the latter incorporated their findings into their final curve of growth. These workers found a general increase of the continuous opacity with wavelength, also shown by the empirical absorption coefficients of Pierce and Waddell (1961) obtained from limb-darkening observations.

We have chosen not to allow for the variation of the continuous-absorption coefficient with wavelength in our empirical curve of growth. The work of Pierce and Waddell shows that for a temperature of 5143° K the variation of $dT/d\tau_\lambda \sim \kappa_\lambda$ is small for $4200 < \lambda < 6800$ which includes the majority of our lines. We have also kept in mind the use of our curve of growth in the analysis of abundances in stars, where it is not the general practice to make such wavelength-dependent corrections. Indeed, for the later spectral types it is difficult to know how to make them. We feel that, if these corrections are not made for stars, the solar curve of growth used in the analysis need not contain them either.

In spite of the fact that our final results do not allow for the variations of κ with wavelength, we have investigated the phenomenon in the same manner as Pierce and Goldberg did. Table 4 shows the mean values of the deviations of the points from our curve of growth as a function of wavelength. The values in the third column give the mean deviations measured in the horizontal direction (in the sense of a change in the effective thickness of the reversing layer) and are designated as $\langle \Delta \log X_{Cr} \rangle$ (see Fig. 6). The fourth column gives the mean deviation from the curve of growth in the vertical direction and is designated as $\langle \Delta \log F \rangle = \langle \Delta (\log W/\lambda + 6.0) \rangle$. The agreement of our results with those of Pierce and Goldberg and of ten Bruggencate is only qualitative.

Let us finally discuss the dependence of an abundance analysis upon the curve of growth from which the solar f-values were obtained. The data available for the analysis of stellar spectra force one to work predominantly with the "flat" and damping portions of the curve of growth. With the resolution generally available in stellar spectroscopy,

the accuracy of the equivalent widths of weak lines is quite low. Abundance determinations are, therefore, more sensitive to the ionization temperature and Doppler width (turbulence) than they are to the exact form of the curve of growth from which the solar f-values were obtained (Aller and Greenstein 1960). New solar f-values may influence the determination of these critical parameters in a way that may only be determined by the use of the new data themselves.

When we compare our curve of growth with those of Pierce and Goldberg (1947) and Wright (1948), which are perhaps the two curves most used in abundance determinations, our curve is somewhat steeper than either. For the elements that span the intermediate or transition portion, the systematic difference between the results obtained

TABLE 4

WAVELENGTH-DEPENDENT DEVIATIONS FROM THE MEAN CURVE OF GROWTH

Wavelength Region (Å)	No of Lines	$\langle \Delta \log X_{Cr} \rangle$	$\langle \Delta \log F \rangle$
3900–4100	52	−0 03	+0 02
4100–4300	67	− 02	+ 02
4300–4500	78	− 05	+ 02
4500–4700	72	+ 01	+ 01
4700–4900	55	− 08	+ 04
4900–5100	29	− 06	+ 03
5100–5300	54	+ 04	− 02
5300–5500	60	− 07	+ .01
5500–5700	35	+ 05	− .02
5700–5900	21	+ 05	− 05
5900–6100	19	+ 16	− 15
6100–6300	34	+ 18	− 10
6300–6500	20	+ 21	− 08
6500–7000	16	+0 15	−0 09

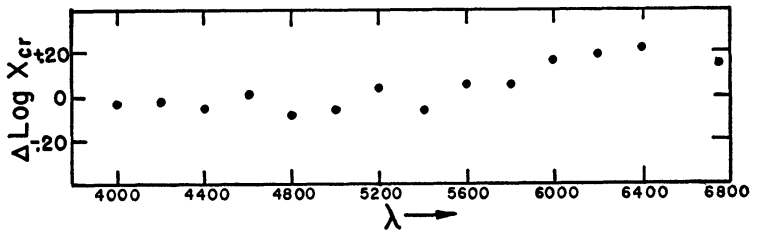

FIG. 6.—Normal points giving the wavelength dependence of the mean deviations of the absorption lines from the empirical curve of growth.

with our curve and the other two will be small. However, if the stellar lines are heavily weighted toward regions where the curvature of our curve is greater, smaller differences in the abundances between the star and the Sun will result.

IV. CONCLUSIONS

We have made a new solar curve of growth chiefly because we felt that the basic data now available (photoelectrically determined equivalent widths and relative f-values extending to high-excitation lines) represented a significant advance over the older material. We thus wished to make these data available for use in the quantitative analysis of stellar atmospheres.

The changes introduced by the new data in the form of the curve may result in different abundances relative to the Sun because of two effects: (i) the transition region of our curve of growth turns more abruptly into the damping portion introducing smaller solar f-values for the strongest lines; (ii) the critical atmospheric parameters ($T_{\rm ion}$, $T_{\rm ex}$, and ξ_t) depend strongly on the resulting stellar curve of growth.

The effect of (i) will in general be small, though systematic, depending on both the number and the distribution of points along the stellar curve of growth. We cannot at present estimate the extent of (ii), but we would like to emphasize the importance of a careful determination of these parameters on the entire abundance analysis.

We could not have even begun this work without the kind help of Dr. E. Müller, who supplied most of the solar equivalent widths. We would also like to thank Dr. O. Mohler and Dr. H. Prince for allowing us to measure equivalent widths of strong lines from the McMath-Hulbert tracings and for helping us in many other ways. Our thanks are due to Mr. J. Tapscott and Mrs. L. Niznik for their help in the preparation of the figures and tables. This research was supported in part by a grant from the National Science Foundation to the University of Chicago.

APPENDIX

It does not appear to be generally recognized that the van de Held curves are the appropriate curves for the schematic model SS–pure absorption, when the equivalent widths are derived from the specific intensity (Sun). We therefore present the following formal justification for the use of these curves; we shall follow the notation of Unsöld (1955). The line depth r_ν may be written in its most general form as

$$r_\nu(\theta) = \int_0^\infty g_1(\tau, \theta)\, e^{-\tau_\nu \sec\theta} d\tau_\nu \tag{A1}$$

(this is Unsöld's eq. [109.4]). If we write $d\tau_\nu = (\kappa_\nu/\kappa)d\tau$, where κ_ν and κ are the line and continuous opacities, and τ_ν and τ are the optical depths that arise from these opacities, this equation becomes

$$r_\nu(\theta) = \int_0^\infty \frac{\kappa_\nu}{\kappa}\, g_1(\tau, \theta)\, e^{-\tau_\nu \sec\theta} d\tau\,. \tag{A2}$$

According to the assumptions of the SS model, however, κ_ν exists only in an infinitesimally thin layer of optical depth x_1 in the line *plus* continuum. Thus we have $d\tau = [\kappa/(\kappa + \kappa_\nu)]dx_\nu \equiv \gamma dx_\nu$ for $0 < x_\nu < x_1$ and $0 < \tau < \tau_1$, where τ_1 is the optical depth in the continuum which corresponds to x_1. We now let τ_1 and γ go to zero in such a way that $x_1 = \tau_1/\gamma$ remains finite. The expression (A2) then becomes

$$r_\nu(\theta) = \int_0^{x_1} g_1(\tau, \theta)\, e^{-\tau_\nu \sec\theta} (1 - \gamma)\, dx_\nu\,. \tag{A3}$$

Within the interval $0 < x_\nu < x_1$ we may take the weighting function $g_1(\tau, \theta)$ to be constant and equal to its value at $\tau = 0$, $g_1(0, \theta)$. We also put $\tau_\nu = [\kappa_\nu/(\kappa + \kappa_\nu)]x_\nu = (1 - \gamma)x_\nu$ and, since $\gamma \to 0$ for $x_\nu < x_1$, equation (A3) may be integrated to yield

$$r_\nu(\theta) = g_1(0, \theta)\, \frac{1}{\sec\theta}\,[1 - \exp(-x_1 \sec\theta)]\,. \tag{A4}$$

If we now introduce the expression for the weighting function at $\tau = 0$ (cf. Unsöld's eq. [101.50]), we obtain

$$g_1(0, \theta) = \left[1 - \frac{(1 - \delta)B(0)}{I_0(0, \theta)}\right] \sec\theta\,. \tag{A5}$$

$B(0)$ is the Kirchhoff-Planck function and $I_0(0, \theta)$ is the specific intensity in the continuum at $\tau = 0$; δ is the *extinction* coefficient for the reversing layer $x_\nu < x_1$. If we take $\delta = 1$ within the reversing layer (pure extinction, no re-emission in the lines) we have precisely the situation of the absorption tube. For $0 < \delta < 1$ we may avoid the question of the assignment of the values of $B(0)$, $I_0(0)$, and δ itself if we write

$$r_\nu(\theta) = r_0(\theta)[1 - \exp(-x_1 \sec\theta)], \tag{A6}$$

where $r_0(\theta)$ is the limiting line depth for the strongest lines. Since $r_0(\theta)$ will be independent of ν, we will have

$$\log W_\nu = \log \int r_\nu d\nu = \log r_0(\theta) + \log \int (1 - e^{-x_1 \sec\theta})\, d\nu\,. \tag{A7}$$

Thus, apart from an additive constant, the curves of growth for the combination SS–pure absorption (specific intensity) will be those given by van de Held for the absorption tube.

We note in passing that (A7) will lead to an expression for the ordinate of the theoretical curve of growth of the form $\log [W_\lambda/(\Delta\nu_D r_0)]$ (cf. Hunger [1956], where the curve of growth for the SS–pure absorption case is given for the flux rather than the specific intensity). The derived Doppler width, and therefore the turbulence, will depend upon the value of r_0. In the Sun $r_0 > .9$ for the stronger lines, and the influence on the derived value of $\Delta\lambda_D$ or $\Delta\nu_D$ is within the errors of fitting the empirical to the theoretical curve. We have simply taken r_0 to be unity in our derivation of ξ_t.

REFERENCES

Allen, C. W. 1934, *Mem. Comm. Sol. Obs. Canberra*, Vol. **1**, No. 5.
———. 1938, *ibid.*, Vol. **2**, No. 6.
Aller, L. H., and Greenstein, J. L. 1960, *Ap. J. Suppl.*, **5**, 139.
Bruggencate, P. ten. 1944, *Zs. f. Ap.*, **23**, 119.
Bruggencate, P. ten, and Houtgast, J. 1941, *Zs. f. Ap.*, **20**, 149.
Corliss, C. H., and Bozman, W. R. 1962, *N.B.S. Monographs*, No. 53.
Held, E. F. M. van de. 1931, *Zs. Phys.*, **70**, 508.
Hunger, K. 1956, *Zs. f. Ap.*, **39**, 38.
Jager, C. de. 1959, *Handbuch der Physik*, ed. S. Flügge (Berlin: Springer-Verlag), **52**, 80.
King, R. B., and King, A. S. 1935, *Ap. J.*, **82**, 377.
———. 1938, *ibid.*, **87**, 24.
Minnaert, M. 1953, *The Sun*, ed. G. P. Kuiper (Chicago: University of Chicago Press).
———. 1960, *Rech. Astr. Obs. Utrecht*, Vol. **15**.
Müller, E. A., and Mutschlecner, J. P. 1964, *Ap. J. Suppl.*, **8**, 1.
Pierce, A. K., and Goldberg, L. 1947, Quarterly Progress Report, October, Office of Naval Research, Project M720–5. (cf. Aller, L. H. 1953, *Atmospheres of the Sun and Stars* [New York: Ronald Press Co.]).
Pierce, A. K., and Waddell, J. H. 1961, *Mem. R. Astr. Soc.*, **68**, 89.
Unsöld, A. 1946, *Zs. f. Ap.*, **24**, 309.
———. 1955, *Physik der Sternatmosphären* (2d ed.; Berlin: Springer-Verlag).
Wright, K. O. 1948, *Pub. Dom. Ap. Obs. Victoria*, **8**, 1.
Wrubel, M. H. 1950, *Ap. J.*, **111**, 157.
———. 1954, *ibid.*, **119**, 51.